# 4-Pentenoyl-isoleucyl-chitosan oligosaccharide and acrylamide functional monomer-dependent hybrid bilayer molecularly imprinted membrane for sensitive electrochemical sensing of bisphenol A†

Qing Gao, Yang Zang, [ID] * Ju Xie, [ID] Yongchuan Wu and Huaiguo Xue*

In this work, an electrochemical sensor was designed for trace monitoring of bisphenol A (BPA) by decorating a hybrid bilayer molecularly imprinted membrane (MIM) on a multi-walled carbon nanotube-modified glassy carbon electrode. When BPA in the MIM was eluted, a composite molecularly imprinted electrochemical sensor was constructed. Under optimal conditions, the developed sensor showed two linear relationships between $\Delta I_p$ and BPA concentration in the range of 0.04 μM to 8 μM, as well as good selectivity and stability, and was also applied to detect BPA in water samples with desirable recoveries ranging from 92.0% to 107.0%.

## Introduction

As an important organic compound with a wide range of applications, bisphenol A (BPA) (Scheme S1†) has been broadly applied in the production of polycarbonate, epoxy resin and other polymer materials,[1] which can be used in many plastic materials contacted in daily life, such as water bottles, baby bottles, food containers and dental sealants. Recent research has demonstrated that BPA can act like estrogen to interfere with the body's endocrine system,[2] inducing abnormal differentiation of reproductive organs and affecting the body's metabolism even at a trace level because its enrichment effect occurs with the migrating from plastic containers to water or food products.[3] Many countries and organizations around the world have restricted the use of BPA in baby products.[4] Therefore, it is indispensable to establish efficacious methods for sensitive detection of BPA in environmental monitoring, food safety and toxicity assessment.

Recently, several analytical methods, such as high-performance liquid chromatography, liquid chromatography-mass spectrometry, gas chromatography-mass spectrometry, surface enhanced Raman scattering, fluorescence and enzyme-linked immune sorbent assay, have been developed for BPA detection.[5–10] However, they still have some deficiencies, including high turnaround time, cumbersome pretreatment, false positive reaction and high cost, which inspires researchers to develop advanced BPA sensing devices. Fortunately, with the rapid progress of nanotechnology and material science, electrochemical sensors have attracted more and more attention because of their superiority in high sensitivity, simple instrument and minimal sample preparation. And many studies on the electrochemical determination of BPA have been reported as expected.[11–13] For example, Wang *et al.* fabricated a mesoporous silica-based electrochemical sensor for sensitive determination of environmental hormone BPA, and the linear range from 0.22 μM to 8.8 μM was obtained with a detection limit of 0.038 μM.[14] To further improve the sensor's detection selectivity, researchers have tried to combine various technologies with electrochemical methods.

Molecularly imprinted polymers (MIPs), prepared by molecularly imprinted techniques, have high potential in electrochemical sensors due to their facile fabrication methods and the specific recognition of template molecule.[15] For example, Haydar Ali *et al.* fabricated a molecularly imprinted polymer nanocomposite electrochemical sensor for selectively detecting BPA in the presence of various BPA analogues, which achieved the linear concentration range from 0.02 μM to 1.0 μM and a detection limit of 8 nM.[16] Sahar Dadkhah *et al.* developed an electrochemical sensing of BPA based on amino-functionalized graphene oxide and molecularly imprinted polymer, displaying two typical linear ranges.[17] Obviously, the construction of an effective molecular imprinted recognition element is the key to the preparation of molecularly imprinted electrochemical sensors (MIES).

In MIPs, the functional monomers with stronger molecular effects on template molecules can be conducive to the enhanced specific recognition of MIPs on target molecules. Commonly used functional monomers, such as acrylic acid and acrylamide, usually interact with the polar parts of the template molecule

*School of Chemistry and Chemical Engineering, Yangzhou University, Yangzhou, Jiangsu, 225002, P. R. China. E-mail: zangyang@yzu.edu.cn; chhgxue@yzu.edu.cn*

only through their polar groups (carboxyl group or amide group). If the spatial structure of a functional monomer well matches the spatial structure of template molecule, that is, the more sites it interacts with, the higher the specificity of functional monomer will be. In order to construct a functional monomer with strong specificity, pentene acyl-amino acyl-chitosan oligosaccharides (PAACO), that matched with the molecular structure of BPA, was prepared by the covalent attachment between the residues of amino acids and the polar groups of chitosan oligosaccharide (Scheme S2†). In particularly, the suitable amino acid residues can be screened out from common neutral amino acids based on quantitative calculation, and benefit to the higher specificity of the optimized oligomer.

In MIES designs, the MIP-based molecularly imprinted films were usually fixed on electrode surface due to the superior properties of the membrane, such as improving the adsorption capacity and mass transfer binding kinetics of the template molecule, and reducing the heterogeneity of the MIP. However, when PAACO is used in the MIM (especially prepared by bulk polymerization), the high permeability of the MIM results in the enhanced entry of template molecules due to the rigid substructure of chitooligosaccharide, but the sensitivity of the MIM decreased. In order to solve this problem, we propose a feasible strategy, that is, taking advantage of the controllable thickness of the electrochemical polymerization film,[18,19] the polymer will be formed by electrochemical polymerization in the gap of the above highly permeable film. As long as the template molecules are insoluble in the polymer solution, the generation of the polymer can well improve the sensitivity of the MIM toward the template molecules.

In addition, to further improve the sensitivity of MIES, a proven effective strategy is to modify the electrode materials with high conductivity, such as graphene and multiwalled carbon nanotubes (MWCNTs), platinum nanoparticle, gold nanoparticles. Among them, MWCNTs is a kind of one-dimensional quantum material with radial size of nanometer and axial size of micron order of magnitude, and both ends of the tube basically sealed.[20] Compared with the other carbon nanocomposites, the introduction of MWCNTs not only easily achieve the capture probe molecules because of their coiled structure and strong π–π electronic interactions,[21,22] but also largely amplify the electrochemical signal due to their high conductivity and large surface area.[23,24] Furthermore, MWCNTs can also effectively increase the number of molecular recognition sites that close to the conducting site in the MIM. Thus, an advanced electrochemical sensing device may be developed by the combination of molecularly imprinted membrane and MWCNTs.

In this work, we selected functional monomer, 4-pentenoyl-isoleucyl-glucosamine (PIGA), with strong interaction on BPA through quantitative calculation, and prepared a permeable MIM by *in situ* bulk polymerization on MWCNTs modified glassy carbon electrode (GCE) by using 4-pentenoyl-isoleucyl-chitosan oligosaccharide (PICO) as a functional monomer oligomer, BPA as a template and ethylene glycol dimethacrylate (EGDMA) as a crosslinking agent. Then, a composite bilayer MIM could be fabricated by electrochemical polymerization of

acrylamide (functional monomer) with the aid of template BPA and crosslinking agent methylene diacrylamide (Scheme 1). After the elution of BPA template from bilayer MIM, a novel BPA electrochemical sensor (denoted as BPA-MIM(MIPs)/MWCNTs/GCE) was fabricated successfully. Besides, differential pulse voltammetry (DPV) was used to investigate the electrochemical behaviour of BPA at the modified electrodes. The experimental parameters affecting the sensitivity of designed sensor were optimized. The analytical application and selectivity behaviour of the sensor were also determined.

## Experimental section

### Materials and reagents

BPA, 4,4′-dihydroxybiphenyl (DHBP), ferulic acid (FA), chloramphenicol (CAP), quercetin (QCT), *N,N*′-methylene bisacrylamide (MBA), 4-pentenoyl chloride, acrylamide (AA) and EGDMA were from Aladdin Reagents (Shanghai) Co., Ltd. COS (average molecular weight 1000–1500) was purchased from Zhejiang Golden·Shell Pharmaceutical Co. Ltd. (Yuhuan, China). 1-Ethyl-3-(3-dimethylaminopropyl) carbodiimide hydrochlorid (EDAC), azobisisobutyronitrile (AIBN), acetic acid, ferrocenemethanol (FCM), *N,N*-dimethylformamide (DMF), dioxane (DO), methanol, ammonium persulfate (APS), sodium acetate and other reagents were purchased from Sinopharm Chemical Reagent Co., Ltd. (Shanghai, China). Multi-walled carbon nanotubes were purchased from Jiangsu Xianfeng Nanomaterial Technology Co., Ltd. EGDMA was distilled under vacuum to remove the inhibitors before usage. DMF was dehydrated with anhydrous magnesium sulfate. All the other chemicals were analytical grade and used as received. All aqueous solutions were prepared using deionized water from a Millipore water purification system (≥18 MΩ cm, Milli-Q, Millipore).

### Solutions preparation

A stock solution of BPA (10 mM) was prepared in (3 : 7, v/v) dioxane: 0.3 M NaAc/HAc (pH 6.5), and other concentrations of BPA solutions could be obtained by diluting BPA solution with 0.3 M NaAc/HAc (pH 6.5) solution. The other assays like BPS, FA, chloramphenicol (CP) and quercetin (QCT) in selectivity test were prepared by a similar method. All the solutions were stored in a refrigerator and protected from lighting.

### Synthesis of PICO

First, 138 mg of $K_2CO_3$ and 131 mg of L-isoleucine were dissolved together in 5 mL water and cooled to 0 °C. Next, 120 mg of 4-pentenoyl chloride was added into the mixture above drop by drop within 10 min. Then, the reactant solution was naturally heated to room temperature under stirring and was continuously stirred for 3 h. 200 mg of EDAC and 160 mg of COS were added into the reaction liquid in order, and the reaction was allowed to proceed for 24 h at room temperature under stirring. After the reaction liquid was precipitated with anhydrous ethanol, the product PICO was centrifuged and dried for further use.
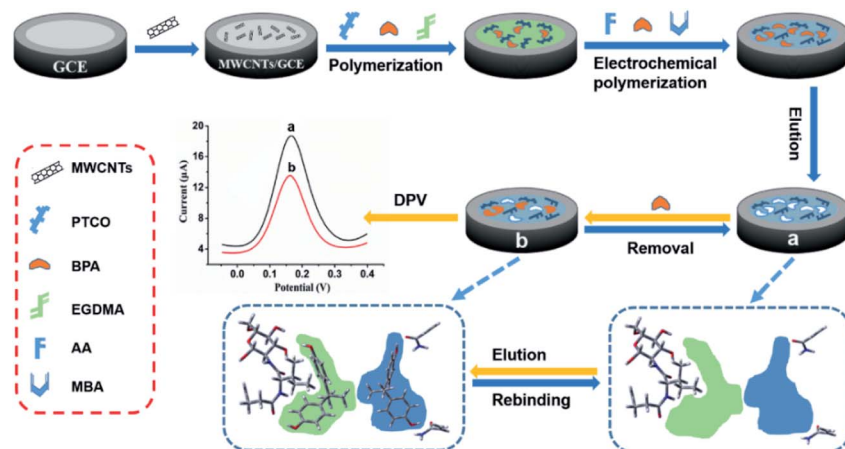
**Scheme 1** The fabrication and detection procedures of designed electrochemical sensor based on the hybrid bilayer molecularly imprinted membrane of BPA.

### Preparation of different modified electrodes

Prior to modification, GCE was polished by 1.0 μm, 0.3 μm and 0.05 μm α-Al$_2$O$_3$ powders in succession and washed with deionized water between each polishing step. After that, GCE was sonicated three times in deionized water and ethanol, respectively, and dried in air. The construction of electrochemical sensor consisted of three steps as follow:

First, MWCNTs were dispersed in DMF by ultrasonication for 1 h to get a homogenous suspension (0.2 mg mL$^{-1}$).[25] Then, 4 μL of MWCNTs suspension was dropped onto freshly polished GCE surface and dried in air, the obtained electrode was marked as MWCNTs/GCE.

Second, the preparation of BPA-dual molecularly imprinted films on GCE was accomplished by a two-step polymerization process. Briefly, 8.4 mg of PICO and 4.41 mg of BPA were dissolved in 2.5 mL water and 2.5 mL DMF respectively, and mixed together. Then 85 μL of EGDMA and 0.5 mg AIBN (initiator) were added into the solution in turn. Place the reaction solution in the refrigerator and take it out after 5 h. Then the mixture was degassed with nitrogen for 5 min. Next, 5 μL of the solution was dropped on the center of the MWCNTs/GCE surface and a clean cover glass was used to cover the droplet. After that, the modified GCE was placed in a reactor and reacted at 65 °C for 8 h, then the primary modified electrode, called as BPA-MIM/ MWCNTs/GCE, was obtained after peeling the cover glass gently.

Third, the secondary imprinting process was accomplished by electrochemical polymerization in an electrolyte containing 13 mg N,N′-methylene bisacrylamide (MBA), 0.11 mg acrylamide, 0.10 mg BPA and 1.2 mg ammonium persulfate (APS) in 1 mL of 0.3 M NaAc solution (pH 6.5), which was performed by cyclic voltammetry (CV) for 6 cycles on the BPA-MIM/MWCNTs/ GCE, and the scanning potential ranged from −1.2 V to 0 V with a scan rate of 20 mV s$^{-1}$.[26] The resulting electrode was marked as BPA-MIM(MIPs)/MWCNTs/GCE. If only MBA is used in this process, the prepared electrode was called as BPA-MIM (PM)/ MWCNTs/GCE.

Finally, the BPA-MIM(MIPs)/MWCNTs/GCE was soaked in the methanol solution containing 30% acetic acid under stirring for 25 min at room temperature to extract BPA molecules. For comparison, non-imprinted membrane (NIM) and non-molecularly imprinted polymers (NIPs) modified MWCNTs/ GCE (denoted as NIM(NIPs)/MWCNTs/GCE) was also prepared in the same way without BPA. All sensors were preserved in a dryer.

### Electrochemical measurements

CV and DPV characterization of the sensor were carried out in 5 mL of acetic acid buffer (0.3 M, pH 6.5) containing 1.0 mM FCM by employing different modified electrodes, saturated calomel electrode (SCE), and platinum wire electrode as the working, auxiliary, and reference electrodes, respectively. The potential range and scan rate were −0.2 V to +0.5 V and 100 mV s$^{-1}$ for CV measurements, and the relevant parameters were set to −0.05 V to 0.45 V with a pulse width, pulse period, and quiet time of 0.0167, 10, and 10 s for DPV measurements. The electrode was regenerated by continuous elution with a methanol solution containing 30% acetic acid under stirring for 25 min to remove BPA from the sensor after each test.

## Results and discussion

### Analysis of quantitative calculation results

The interaction energies between the functional monomers and BPA, calculated in gas phase for all complexes formed, were summarized in Table S1.† The results showed that the binding energy of 4-pentenyl-isoleucinyl-glucosamine (PILEGA)-BPA complex could reach −99.42253902 kJ mol$^{-1}$, which is the lowest among all complexes. This suggested that PILEGA could form a more stable complex with BPA.[27] Thus, PILEGA can be used as a functional monomer, *i.e.*, its oligomer (PICO) can be used as the functional monomer oligomer in this study.

The optimized geometries of BPA, PILEGA and their complex was showed in Fig. 1. In the molecular complex, two phenolic hydroxyl groups from BPA could form two hydrogen bonds with
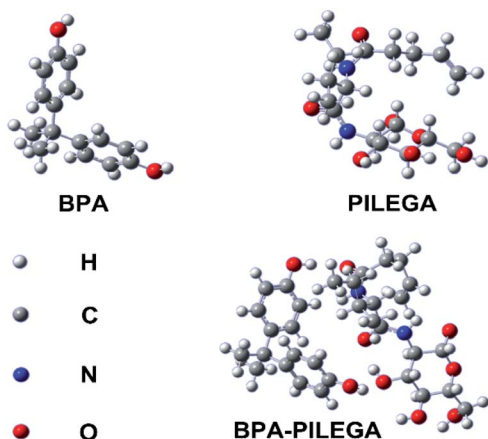
**Fig. 1** Optimized conformations of the most stable complexes of BPA with PILEGA derived by Hartree–FockFig method with 6-31G(d) basis set.

the hydroxyl group in the third carbon of the pyranose ring and the carbonyl oxygen of the pentenyl group, respectively. Besides, the presence of side chain residues in the isoleucine portion of the monomer makes the complex more stable. More information on the quantitative calculations can be available in the ESI.†

## Characterization of PICO

The FTIR characteristic peaks of PICO was displayed in Fig. 2A. From the spectrum, the broad band near at 3340 cm⁻¹ corresponded to stretching vibration deformation of O–H and N–H bond on the oligosaccharide and the amino group on the amide group. The characteristic peaks at 2929–2883 cm⁻¹ assigned to the stretching vibration of C–H bond in methyl and methylene groups. The absorption peaks, suited at 1651 cm⁻¹ and 1561 cm⁻¹, were mainly attributed to –CONH. Besides, SEM-EDS testing was used to analyze the C, N, O elements in PICO sample (Fig. 2B), and the corresponding atom percent were 54.35%, 15.79% and 29.86%, respectively, which was equivalent to the value of the elemental analysis (C: 54.48%, N: 7.48%, O: 29.98%). These results proved that the synthesis of PICO was successful.

## Optimization of the first molecular imprinting experimental conditions

First, the effect of the amount of PICO on the permeability of the MIM was investigated through the different proportions of
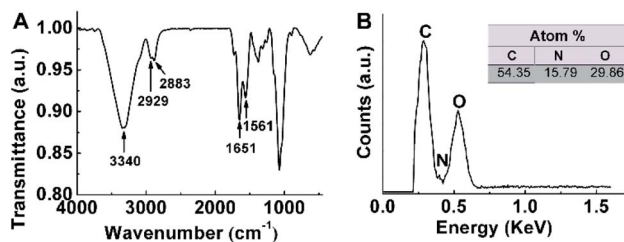
PILEGA (as the monomer of PICO) and cross-linking agent (EGDMA). According to CV measurements (Fig. S1†), the oxidation peak current of FCM raised gradually with the increment of PILEGA content in the polymer film on GCE surface, suggesting the increase of membrane's permeability.

When the PILEGA ratio was at 5 : 100, the permeability of the film arrived at the peak value. Thereafter, the permeability reduced slowly with the increasing of film thickness. Therefore, the ratio of PILEGA to EGDMA in bulk polymerization was set as 5 : 100 to reduce the influence of membrane thickness in the subsequent experiment.

Second, the influence of various BPA/PILEGA ratios (2 : 5, 2.5 : 5, 3 : 5, 3.5 : 5, 4 : 5) on sensor performance in bulk polymerization was surveyed under the conditions described above except BPA in the second polymerization process (Fig. S2†). When the BPA/PILEGA ratio was at 3.5 : 5, the DPV of the sensor achieved the highest current response, whereas the other sensors prepared with more or less BPA had a relatively weak DPV response. These results indicated that the imprinting sites generated by removing of BPA in the MIM increased with the increase of BPA before the molar ratio 3.5 : 5, and decreased after this value. This may attribute to the insolubility of BPA in water, and abundant BPA molecules could impede the generation of the electrochemical polymer in the interior of primary MIM. So, the optimum BPA/PILEGA ratio was 3.5 : 5.

## Optimization of the second molecular imprinting experimental conditions

The purpose of the secondary imprinting is to improve the sensitivity of the primary imprinted film, so the thickness and permeability of the secondary imprinted film should be equal to that of the secondary polymerized film. To investigate the performance of the secondary polymerization film, the optimal concentration of MBA in polymerization process should be investigated first (Fig. S3†). When MBA concentration was 11.5 mg mL⁻¹, the prepared BPA-MIM(PM)/MWCNTs/GCE had the highest DPV response, while DPV response of the sensor at other MBA concentrations was relatively small. This result indicated that the obtained secondary polymeric film was suitable for the sensor when the concentration of MBA was 11.5 mg mL⁻¹. Thus, the electrochemical performance of the second imprinted film should be similar to that of the secondary polymeric film.[28]

For an electrochemical reversible process, the electrode performance was often investigated by the relationship between the peak current and the scanning speed using cyclic voltammetry. Refer to the Randles–Sevcik formula:[29]

$$I_p = 0.4463 \times (F^3/RT)^{1/2} \times n^{3/2} \times A \times D_0^{1/2} \times Cv^{1/2} \quad (1)$$

where $I_p$ is the peak current value, $F$ is Faraday constant (96 480 C mol⁻¹), $T$ is temperature (K), $R$ is gas constant (8.314 J K⁻¹ mol⁻¹), $n$ is number of electrons transferred in the redox event (usually 1), $A$ is electrode area (cm²), $D_0$ is diffusion coefficient (cm² s⁻¹), $C$ is concentration (mol cm⁻³) and $u$ is scan rate (V s⁻¹). According to formula (1), under similar conditions, the electrochemical performance of two different modified



**Fig. 2** (A) The infrared spectra and (B) energy-dispersive spectrometry of PICO. The table data inserted in panel B is the result of PICO element analysis.

electrodes depends on the electrode area. For the process of diffusion control, formula (1) can be summarized into formula (2).

$$I_p/\nu^{1/2} = KAC \tag{2}$$

In this formula,

$$K = 0.4463 \times (F^3/RT)^{1/2} \times n^{3/2} \times D_0^{1/2} \tag{3}$$

According to formula (2), the effective area of the electrode should be proportional to the slope of the $I_p$–$\nu^{1/2}$ curve.

The relationship between peak current ($I_p$) and square root of scan rate ($\nu$) of polymeric film electrode, formed by MBA solution at different concentrations, was recorded by CV curves. As shown in Fig. S4,† $I_p$ had a linear relation with $\nu^{1/2}$, and the higher the MBA concentration, the smaller the slope of $I_p$–$\nu^{1/2}$ curve.[30,31] These results indicated that the membrane electrode was affected by diffusion control. Its performance was related to the effective area of the electrode, and the higher the concentration of MBA would lead to lower the effective area of the membrane electrode.

In the secondary printing process, MBA was used as cross-linking agent, acrylamide as functional monomer, BPA as the template molecule. Since the freedom degree of acrylamide polymerization was 2 and that of MBA was 4, the cross-linking degree of the polymer formed by copolymerization process was lower than that of MBA. Therefore, to achieve the electro-chemical performance of secondary imprinted film, the concentration of MBA in the secondary imprinted polymer solution must be increased.

The amount of BPA also had a great effect on the electro-chemical properties of the secondary imprinted film. Fig. S5† indicated the relationship between CV $I_{pa}$ and $\nu^{1/2}$ of polymeric film electrode at 13 mg mL$^{-1}$ MBA and different BPA concentrations. The addition of more BPA into polymerization solution resulted in the higher slope of $I_p$–$\nu^{1/2}$ curve. When the concentration of BPA was at 0.1 mg mL$^{-1}$, the slope was less than that of the secondary polymerization film. If acrylamide was added in this case, the slope for the secondary imprinted film would be increased to the slope of the secondary polymeric film again.

The relationship between CV $I_{pa}$ and $\nu^{1/2}$ of polymeric film electrode at different AA/BPA ratios (3.5 : 1, 3.75 : 1, 4.0 : 1) (Fig. S6†) showed that the slop of $I_p$–$\nu^{1/2}$ curve at 3.75 : 1 was close to that of the secondary polymer film. Thus, the concentrations of MBA and BPA in the secondary imprinted polymerization solution were 13 mg mL$^{-1}$ and 0.1 mg mL$^{-1}$, respectively, and the ratio of AA/BPA was selected as 3.75 : 1.

The scanning cycles of CV in the process of secondary imprinting also has a great influence on the performance of the polymer film. The relationship between $I_p$ and $\nu^{1/2}$ of secondary imprinted film electrode prepared at different scanning cycles ($n = 5, 6, 7$) was recorded in Fig. S7,† which indicated that the slop of $I_p$–$\nu^{1/2}$ curve at 6 scanning cycles was the closest to that of the secondary polymerization membrane. Fig. S8† further confirmed the effect of CV scanning cycles on the performance of designed sensor. When the scanning number was at 6, the

maximum of $\Delta I_p$ was observed. Meanwhile, as shown in Fig. S9,† the continuous scanning of electrochemical sensor enabled the declined DPV response, accompanied by the increase of secondary imprinting film thickness. When the number of scan cycles reached the 6th cycle, the obtained CV curve had little change compared to the shape of the 5th cycle. Based on this, the scanning cycles of CV was set at 6.

### Effect of the secondary MIM on test performance

Under optimized conditions, the secondary molecularly imprinted polymerization was carried out on the basis of the primary non-molecularly imprinted membrane, and the performance of the modified electrode (BPA-NIM(MIPs)/MWCNTs/GCE) was tested at different BPA concentrations (Fig. S10A and B†). The results showed that the variation value of DPV peak current can increase with the BPA concentration in the range of 0.5–3 μM. When the BPA concentration reached 2.0 μM, the change value of DPV peak current had closed to the maximum. Although this variation was not large, the secondary imprinting polymerization could also give the composite membrane an enough response to BPA.

### Elution time and incubation time of bilayer MIM

It is a crucial step for sensor's performances to remove BPA molecules from the double-layer MIM. Considering H-bond was the main molecular force between the functional monomer oligomer and BPA, a mixture of methanol and acetic acid was used as the eluent. Since the amide group in the secondary imprinted film was easy to hydrolyze under strong acidity, the ratio of methanol to acetic acid was selected as 3 : 1. More importantly, when BPA elution time in the imprinted film was 25 min, the stability and reproducibility of designed sensor were satisfactory (Fig. S11†). So, methanol/acetic acid (3 : 1, v/v) and 25 min were selected as the eluent and elution time.

To compare BPA-independent DPV responses of the primary imprinted film and composite imprinted film prepared with or without MWCNTs, the incubation time of different modified electrodes was tested in the test solution at 2.0 μM BPA every 3 min. As shown in Fig. S12,† DPV peak current of the primary imprinted film reached the platform region within 10 min (curve a), while the composite imprinted films with (curve b) or without (curve c) MWCNTs took 33 min and 30 min to reach the relatively stable level, respectively. These results illustrated that the primary imprinted film had a relatively fast kinetic process, whereas the adsorption kinetics of the composite imprinted film gradually slowed down. Because the adsorption kinetics has little influence on the adsorption accuracy after 33 min. Thus, 33 min was selected as an optimal incubation time.

### Characterization of different modified electrodes

The SEM images of the modified electrodes at each step were shown in Fig. 3. From the images, MWCNTs were uniformly dispersed on smooth GCE surface (Fig. 3A and B). When MWCNTs modified GCE electrode was wrapped by polymer films, the distribution of MWCNTs were still visible, and the pore structures of the MIM was observed after first
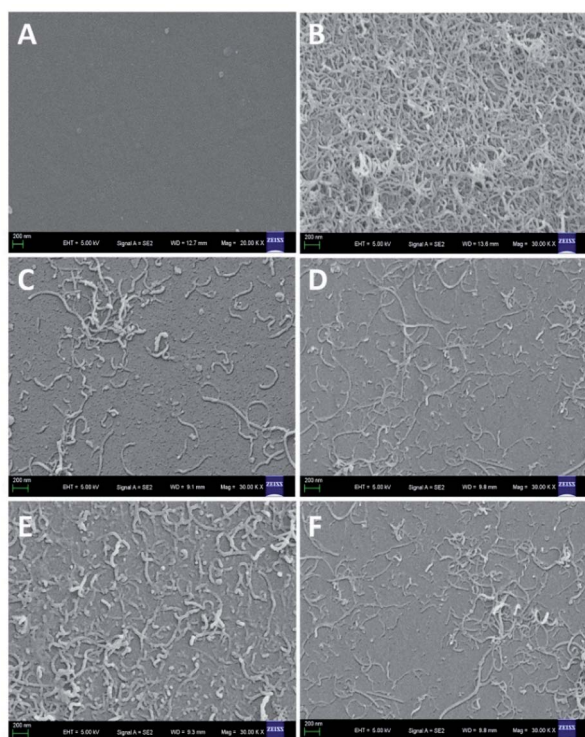
Fig. 3 SEM images of bare GCE electrode (A), MWCNTs (B) and MWCNTs/GCE after bulk polymerization (C), and electrochemical polymerization before (D) and after (E) template removal, as well as NIM/MWCNTs/GCE after leaching process (F).

polymerization (Fig. 3C). However, the generated nanopores were reduced significantly, and the film surface became slightly smooth after the subsequent electrochemical polymerization (Fig. 3D). When BPA template removed, the morphology of MIM became rougher than that before (Fig. 3E). Similar phenomena appeared in the NIM surface (Fig. 3F).

A small amount of MWCNTs, observed on the surface of polymer film, could provide more conductive area for as-prepared electrode. The formed nanopores on MIM surface, ascribed to the nitrogen released by AIBN decomposition, could increase the effective reactive sites and further improve the membrane's permeability.

In the process of secondary imprinted electro-polymerization, MIPs were deposited near the conductive sites in the imprinted film gap, and most of nanopores could be filled by the generated polymer, resulting in a slightly smooth surface. However, the membrane surface resulted from secondary imprinting had no significant change. After eluting the BPA molecules, the number of recognition sites in BPA-MIM complex largely increased, leading to an enhanced sensitivity for electrochemical sensor.

### Electrochemical characterization

Electrochemical behavior of the modified electrodes was investigated by using FCM as a redox probe (Fig. 4). It could be seen from Fig. 4A that there were great differences in the CV

curves of various electrodes. Compared to bare GCE (curve a), the redox peak current increased slightly after being modified by MWCNTs (curve b). This result might be attributed to their large surface area and conductivity of MWCNTs. For BPA-MIM/MWCNTs/GCE, the redox peaks of FCM decreased obviously (curve c), while the peaks were almost invisible as to BPA-MIM(MIPs)/MWCNTs/GCE before template removal (curve d), indicating that the nanopores still presented in the imprinted film after bulk polymerization and then the secondary imprinted film inhibited the FCM molecules access to the electrode surface. After eluting the template BPA from MIPs, the redox peaks increased clearly (curve e). These results suggested that imprinted cavities, produced in the MIM after the removal of BPA molecules, may enhance the diffusion of FCM and facilitate the redox reaction of FCM on electrode surface. However, when BPA was re-absorbed by the sensor, the imprinted cavities were occupied by BPA, leading to the reduction of the redox peak current from curve e to f. For NIM (Fig. 4B), besides, the redox current raised slightly from curve g to curve h after immersing NIM/MWCNTs/GCE in methanol/acetic acid (3 : 1, v/v), because no imprinted cavities were eluted except for the residual initiator decomposed in the membrane.

### Calibration curve of the sensor

Under the optimized conditions, DPV test was utilized to investigate the linearity and detection limit of the bilayer imprinting sensor for BPA. As shown in Fig. 5A, the peak current was inversely proportional to the BPA concentration. Fig. 5B illustrated a corresponding plot, showing two linear relationships between the variation of peak current value ($\Delta I_p = I_0 - I_c$) and BPA concentration in the range of 0.04 to 8 $\mu$M, where $I_0$ and $I_c$ present the peak currents of the sensor at blank sample and other BPA concentrations, respectively. The corresponding linear regression equations were $\Delta I_p = 0.38043 + 4.70753C$ ($\mu$M) ($R = 0.99291$) in 0.04–0.2 $\mu$M and $\Delta I_p = 1.05965 + 0.87814C$ ($\mu$M) ($R = 0.99873$) in 0.2–8.0 $\mu$M.

As a control, sensors without MWCNTs were prepared and the same tests were performed. As displayed in Fig. S13,† there were two linear relationships between peak current and BPA
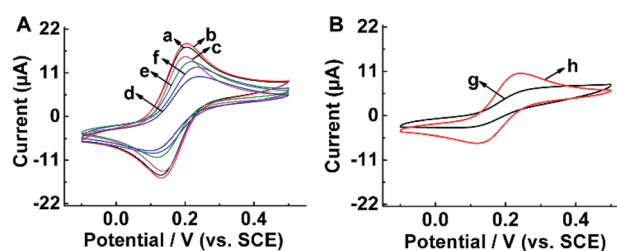


Fig. 4 (A) Cyclic voltammograms of different electrodes: bare GCE (a), MWCNTs/GCE (b), BPA-MIM/MWCNTs/GCE (c), BPA-MIM(MIPs)/MWCNTs/GCE (d), MIM(MIPs)/MWCNTs/GCE after BPA removal (e), MIM(MIPs)/MWCNTs/GCE after BPA rebinding (f); (B) CV responses of different electrodes: NIM(NIPs)/MWCNTs/GCE (g), and (g) after leaching step with 3 : 1 (v/v) methanol/acetic acid (h). Redox probe: 1.0 mM FCM in 0.3 M NaAc/HAc solution (pH 6.5), Scan rate: 100 mV s$^{-1}$.
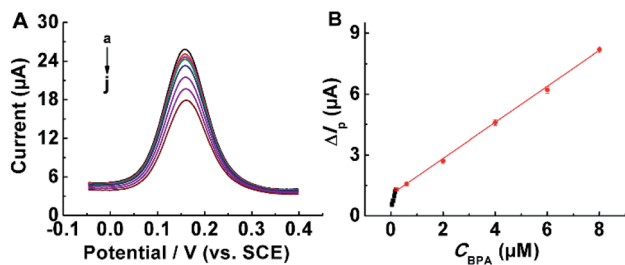
**Fig. 5** (A) DPV of MIM(MIPs)/MWCNTs/GCE in 0.3 M NaAc/HAc solution (pH 6.5) containing 1.0 mM FCM at different BPA concentrations, (a): 0 µM, (b): 0.04 µM, (c): 0.08 µM, (d): 0.12 µM, (e): 0.16 µM, (f): 0.20 µM, (g): 2.0 µM, (h): 4.0 µM, (i): 6.0 µM, (j): 8.0 µM. (B) The corresponding calibration curve. Error bars represent the standard deviation from 3 parallel tests.
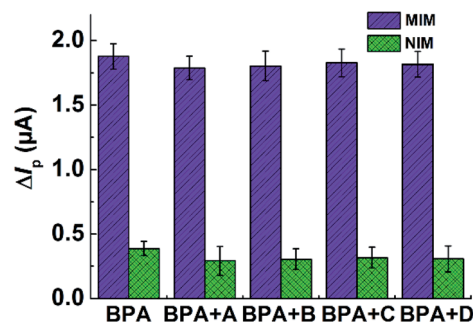


**Fig. 6** The selectivity of the prepared MIM(MIPs)/MWCNTs/GCE and NIM/MWCNTs/GCE in BPA and the mixture of BPA and its analogues at 1.0 µM by DPV: (A) DHBP, (B) FA, (C) CAP, (D) QCT. Error bars represent the standard deviation from 3 parallel tests.

level in the range from 0.04 µM to 8 µM. The corresponding linear regression equations were $\Delta I_p = 0.32725 + 3.85589C$ (µM) ($R = 0.99454$) in 0.08–0.2 µM and $\Delta I_p = 0.89421 + 0.7136C$ (µM) ($R = 0.99866$) in 0.2–6.0 µM, respectively. Obviously, the addition of MWCNTs improved the sensitivity of developed sensor.

The detection limit (LOD) of designed sensor was calculated to be 8 nM (S/N = 3). As a result, the prepared sensors were excellent candidates compared to the other types of MIES for BPA assays. For comparison, several molecularly imprinted BPA sensors with different materials and modifications reported in literature were listed in Table S2.† Compared to other reported sensors, the MIM(MIPs)/MWCNTs/GCE sensor achieved satisfactory sensitivity, acceptable dynamic range and low detection limit due to the introduction of MWCNTs and double-layer molecular imprinting.

It is not difficult to see that, compared with the content in section of the effect of the secondary MIM on test performance, excluding the influence of NIM, the effect of BPA concentration on the response of the sensor after secondary imprinting polymerization was up to 12% in the range of 0.5–2 µM. With the increase of BPA concentration, this effect gradually decreased, which suggested that the performance of the secondary imprinted polymer after adsorption of template molecules was close to that of the secondary polymer film.

### Selectivity, repeatability and stability of the sensor

To evaluate the selectivity of the MIM(MIPs)/MWCNTs/GCE sensor, DPV responses of designed sensor toward 1.0 µM BPA were measured in the presence of the same concentration of DHBP, FA, CAP, QCT as interfering substances. As evident from Fig. 6, the current variation of BPA for proposed sensor was similar to that of mixed samples containing BPA and the other interfering species, whereas the corresponding current change for the NIM/MWCNTs/GCE was very small. So, the designed sensor achieved a favorable selectivity for BPA assay.

Three measurements of MIM(MIPs)/MWCNTs//GCE at 1.0 µM BPA were used to assess the reproducibility of designed electrochemical sensor. The relative standard deviation (RSD) of the sensors was calculated about 3.5%. In addition, the repeatability and stability of the sensors were also evaluated by

**Table 1** Determination of different concentrations of BPA in real samples by using the developed sensor ($n = 3$)

| Sample no. | Added (µM) | Found (µM) | RSD (%) | Recovery (%) |
|---|---|---|---|---|
| Tap water | 0.5 | 0.46 | 4.33 | 92 |
| | 1.0 | 1.07 | 3.85 | 107 |
| | 1.5 | 1.46 | 3.13 | 97.3 |
| | 2.0 | 1.91 | 4.94 | 95.5 |
| Mineral water | 0.5 | 0.53 | 3.48 | 106 |
| | 1.0 | 0.94 | 4.23 | 94 |
| | 1.5 | 1.59 | 3.65 | 106 |

the same way. The sensor sustained more than 90% of the original test value after storage in a sealed capsule at room temperature for 20 days. The RSD of the sensor after 3 continuous scanning was 3.3%. These results displayed that this electrochemical sensor can be reusable and storable.

## Sample analysis

The applicability of the proposed sensor was evaluated in real samples by a standard addition method. Considering that BPA molecule could react with some hydrophobic proteins in milk to form a complex, two real water samples were used for practical testing. In this method, 1 mM BPA solutions was added to water samples to make certain concentrations of BPA (e.g., 0.5 µM, 1.0 µM, 1.5 µM and 2.0 µM). The electrochemical responses were detected by DPV under optimal experimental conditions. As shown in Table 1, the sensor exhibited an excellent recovery ranged from 92% to 107%, and reproducibility expressed as the RSD was less than 5%. These results suggested that our method was convenient for the analysis of practical samples.

## Conclusions

In this study, a functional monomer oligomer, PICO, was successfully synthesized, which exhibited a strong molecular interaction on BPA molecule. Based on this, a novel and sensitive electrochemical molecular imprinting sensor was

developed for accurate detection of BPA by coupling with MWCNTs and hybrid bilayer MIM. Among them, the addition of secondary imprinting polymerization raised its response up to 12% in the range of 0.5–2 μM BPA, and the generation of bilayer molecularly imprinted membrane provided an excellent selectively recognize toward BPA template. Considering its good reproducibility and repeatability, the sensor designed could be utilized to evaluate actual samples in water, showing a great promising in water quality monitoring application.

## Conflicts of interest

There are no conflicts to declare.

## Acknowledgements

## Notes and references

1 J. E. Cooper, E. L. Kendig and S. M. Belcher, *Chemosphere*, 2011, **85**, 943–947.

2 J. X. Shi, C. Y. Liu, M. Y. Chen, J. H. Yan, C. G. Wang, Z. H. Zuo and C. Y. He, *Environ. Toxicol.*, 2020, **36**, 665–674.

3 F. Cariati, N. D'Uonno, F. Borrillo, S. Iervolino, G. Galdiero and R. Tomaiuolo, *Reprod. Biol. Endocrinol.*, 2019, **17**, 1–8.

4 Y. Lin, X. Qiu, J. Liu, C. H. Tseng, P. Allard, J. A. Araujo and Y. Zhu, *Environ. Int.*, 2020, **141**, 105758.

5 M. Rezaee, Y. Yamini, S. Shariati, A. Esrafili and M. Shamsipur, *J. Chromatogr. A*, 2009, **1216**, 1511–1514.

6 N. C. Maragou, E. N. Lampi, N. S. Thomaidis and M. A. Koupparis, *J. Chromatogr. A*, 2006, **1129**, 165–173.

7 M. Del Olmo, A. Gonzalez-Casado, N. A. Navas and J. L. Vilchez, *Anal. Chim. Acta*, 1997, **346**, 87–92.

8 J. Q. Xue, D. W. Li, L. L. Qu and Y. T. Long, *Anal. Chim. Acta*, 2013, **777**, 57–62.

9 L. Molina-García, M. L. Fernández-de Córdova and A. Ruiz-Medina, *Talanta*, 2012, **96**, 195–201.

10 M. Jia, S. Chen, T. T. Shi, C. Y. Li, Y. P. Wang and H. Y. Zhang, *Food Chem.*, 2021, **344**, 128602.

11 P. Hu, X. Zhu, X. Luo, X. Hu and L. Ji, *Microchim. Acta*, 2020, **187**, 1–9.

12 L. A. D. Gugoasa, *J. Electrochem. Soc.*, 2019, **167**, 037506.

13 O. Koyun, S. Gorduk, M. Gencten and Y. Sahin, *New J. Chem.*, 2019, **43**, 85–92.

14 F. G. Wang, J. Q. Yang and K. B. Wu, *Anal. Chim. Acta*, 2009, **638**, 23–28.

15 R. J. Gui, H. Jin, H. J. Guo and Z. H. Wang, *Biosens. Bioelectron.*, 2018, **100**, 56–70.

16 H. Ali, S. Mukhopadhyay and N. R. Jana, *New J. Chem.*, 2019, **43**, 1536–1543.

17 S. Dadkhah, E. Ziaei, A. Mehdinia, T. B. Kayyal and A. Jabbari, *Microchim. Acta*, 2016, **183**, 1933–1941.

18 Y. Ma, X. L. Shen, Q. Zeng and H. S. Wang, *Talanta*, 2017, **164**, 121–127.

19 M. Arvand, M. Zamani and M. S. Ardaki, *Sens. Actuators, B*, 2017, **243**, 927–939.

20 Á. Kukovecz, G. Kozma and Z. Kónya, *Multi-walled carbon nanotubes, Springer handbook of nanomaterials*, Springer, 2013, pp. 147–188.

21 Y. Y. Zhang, W. H. Huang, X. F. Yin, K. A. Sarpong, L. M. Zhang, Y. C. Li, S. Zhao, H. D. Zhou, W. M. Yang and W. Z. Xu, *React. Funct. Polym.*, 2020, **157**, 104767.

22 E. Haghshenas, T. Madrakian, A. Afkhami and H. S. Nabiabad, *J. Iran. Chem. Soc.*, 2019, **16**, 593–602.

23 H. Beitollahi, F. Movahedifar, S. Tajik and S. Jahani, *Electroanalysis*, 2019, **31**, 1195–1203.

24 T. M. Oliveira and S. Morais, *Appl. Sci.*, 2018, **8**, 1925.

25 G. A. M. Ali, E. Megiel, P. Cieciórski, M. R. Thalji, J. Romański, H. Algarni and K. F. Chong, *J. Mol. Liq.*, 2020, **318**, 114064.

26 R. D. da Fonseca Alves, A. G. da Silva, L. F. Ferreira and D. L. Franco, *Talanta*, 2017, **165**, 69–75.

27 C. F. Silva, L. F. Menezes, A. C. Pereira and C. S. Nascimento Jr, *J. Mol. Struct.*, 2021, **1231**, 129980.

28 Q. Gao, Y. Zang, Y. Zhang, J. Xie, J. Y. Li, J. F. Gao and H. G. Xue, *J. Electroanal. Chem.*, 2020, **879**, 114793.

29 M. Zaib and M. M. Athar, *Instrum. Sci. Technol.*, 2018, **46**, 408–425.

30 N. P. Shetti, S. J. Malode, D. S. Nayak, G. B. Bagihalli, K. R. Reddy, K. Ravindranadh and C. V. Reddy, *Microchem. J.*, 2019, **149**, 103985.

31 P. C. Zhu and Y. Y. Zhao, *Mater. Chem. Phys.*, 2019, **233**, 60–67.